Theoretical analysis predicts an optimal therapeutic strategy in distinct parkinsonian landscapes of the striatum

Mathias L. Heltberg[1,2,3], Hussein N. Awada[4,5], Alessandra Lucchetti[2], Mogens H. Jensen[2]*, Jakob K. Dreyer[6]* and Rune Rasmussen[7,8]*

[1] Laboratoire de Physique, École Normale Supérieure, 75231 Paris Cedex 05, France
[2] Niels Bohr Institute, University of Copenhagen, 2100 Copenhagen, Denmark
[3] Center for Infection Control, Statens Serum Institut, 2300 Copenhagen S, Denmark
[4] Section of Surgical Pathophysiology, Rigshospitalet, University Hospital Copenhagen, 2200 Copenhagen, Denmark
[5] Department of Anesthesiology, Centre of Cancer and Organ Diseases, Rigshospitalet, University Hospital Copenhagen, 2100 Copenhagen, Denmark
[6] Department of Bioinformatics, H Lundbeck A/S, 2500 Valby, Denmark
[7] Danish Research Institute of Translational Neuroscience – DANDRITE, Nordic-EMBL Partnership for Molecular Medicine, Department of Biomedicine, Aarhus University, 8000 Aarhus, Denmark
[8] Lead Contact

* Correspondence: mhjensen@nbi.ku.dk; jakd@lundbeck.com; runerasmussen@dandrite.au.dk

Summary

Parkinson's disease (PD) results from a loss of dopaminergic neurons. The age of disease onset, its progression and symptoms vary significantly between patients, pointing to a complex relationship between neuron loss and PD etiology. Yet, our understanding of the clinical variability remains incomplete. Here, we use biophysical modelling to investigate the dopaminergic landscape in the healthy and denervated striatum. Based on currently proposed mechanisms causing PD, we model three distinct denervation patterns, and show notable differences in the dopaminergic network as denervation progresses. We find local and global differences in the activity of two types of striatal neurons as a function of the denervation pattern. Finally, we identify the optimal cellular strategy for maintaining normal dopamine signaling when neurons degenerate within our model. Our results derive a conceptual framework in which the clinical variability of PD is rooted in distinct denervation patterns and forms testable predictions for future PD research.

Introduction

Parkinson's disease (PD) is the second most common neurodegenerative disorder, affecting 1% of people over the age of 60 worldwide (Hirtz et al., 2007). The disease is caused by a progressive loss of dopaminergic neurons in the substantia nigra pars compacta (SNc) (Damier et al., 1999; Rodriguez-Oroz et al., 2009), and symptoms typically emerge when 60–80% of the neurons are lost (Bernheimer et al., 1973; Fearnley and Lees, 1991; Lee et al., 2000; Ma et al., 1997). Notably, the age of onset, disease progression, response to treatment and symptoms are highly variable between patients (Greenland et al., 2018; Lewis et al., 2005), pointing to a complex relationship between neuron loss and PD etiology that remains to be understood.

Dopaminergic SNc neurons send projections to the dorsal striatum in the basal ganglia (**Figure 1A**), an important brain area for motor function and executive control (Graybiel and Grafton, 2015; Kreitzer and Malenka, 2008). These projections promote movement by modulating the excitability of striatal spiny projection neurons (SPNs) by activating D1- or D2-class dopamine (DA) receptors (Kreitzer, 2009; Surmeier et al., 2007). DA increases the excitability of D1 receptor-expressing SPNs (D1-SPNs) and decreases the excitability of D2 receptor-expressing SPNs (D2-SPNs) (Kreitzer, 2009; Kreitzer and Malenka, 2008; Lahiri and Bevan, 2020). D1- and D2-SPNs are critical components of two distinct pathways controlling movement in opposing ways: the direct pathway promotes desired movements while the indirect pathway suppresses unwanted movements (Cui et al., 2013; Freeze et al., 2013; Kravitz et al., 2010; Kreitzer and Malenka, 2008) (**Figure 1B**). In PD, dopaminergic neurons are progressively lost, leading to striatal DA depletion, abnormal SPN activity and movement deficits (Kravitz et al., 2010; Mazzoni et al., 2007; Panigrahi et al., 2015; Rodriguez-Oroz et al., 2009). Despite the central role of failing DA signaling in the etiology of PD, little is known about the nature of striatal DA signaling before and during disease progression, posing a significant obstacle to the development of therapeutic strategies which maintain normal DA signaling in PD patients.

Efforts focused on understanding the molecular cascades resulting in neurodegeneration in PD (Michel et al., 2016) have proposed different mechanisms, including the prion-hypothesis (Chu and Kordower, 2015; Prusiner, 2012) and oxidative stress (Jenner, 2003; Sulzer, 2007). However, little attention has been given to investigating the spatial and temporal patterns of dopaminergic neuron loss. Clinical imaging techniques, measuring DA transporter densities, provide a correlate of dopaminergic innervation (Wang et al., 2012; Wszolek et al., 2015), but cannot resolve the fine-scale organization of dopaminergic neurons within striatal regions. In animal models, neuronal firing and DA signals can be recorded invasively (Lippert et al., 2019; Paladini et al., 2003; Patriarchi et al., 2018) and correlated with dopaminergic neuron density postmortem. In addition to the challenge of being spatially limited to a highly localized area, this approach lacks the temporal scale needed to track slow changes in neuron density and DA signaling.

We have developed biophysical computational models to probe cause-and-effect in a reduced parameter space. By investigating the spatial patterns and processes of DA signaling degeneration, we found that distinct denervation patterns can be characterized by unique temporal evolutions and DA signaling dynamics. We also show that the denervation pattern differentially affects both the local and global activity of D1- and D2-SPNs. Finally, we

demonstrate that an ideal compensatory cellular strategy for maintaining normal DA signaling, despite neuron loss, is to enhance both DA release and DA uptake in parallel. These results support a conceptual framework where the clinical manifestations of PD are rooted in the distinct denervation patterns and, importantly, provide theoretical predictions to be experimentally tested.

Results

Functional and spatial characterization of DA signaling in the healthy striatum

We began our investigation by modelling DA signaling in the fully innervated human striatum, specifically the putamen, which we defined as the healthy state (Dreyer, 2014; Dreyer et al., 2010). We simulated the firing of dopaminergic SNc neurons and described the DA concentration in the extracellular space. For this, we employed a mean-field model describing DA in a subvolume of 10^3 μm^3 (see Methods). Given the estimated density of dopaminergic axonal terminals in the healthy striatum at ~0.1 per μm^3 (Doucet et al., 1986), this volume contains 100 terminals, each of which was considered an individual element. The DA inside the *i*'th subvolume can be approximated as:

$$\frac{dM_i}{dt} = \Delta \cdot \nu \cdot N_i - V_M N_i \frac{M_i}{K_M + M_i} + (D\nabla^2 M_i - \delta M_i)$$

Here M is the DA concentration, Δ is the amount of DA released by a terminal, ν is the neuronal firing frequency, and N is the number of terminals within the subvolume. DA remains active in the extracellular space until it is removed by either transporters or degraded enzymatically (**Figure 1A**), so we modeled transporter-mediated DA uptake after the Michaelis-Menten uptake equation. We also included a simple degradation term, and a term to account for the diffusion between neighboring subvolumes (**Figure 1A**). However, for all but extreme cases, these are relatively negligible and therefore they are placed in parentheses. We assumed that each dopaminergic neuron can express one of two distinct firing patterns: tonic firing, where ν is constant around 4–5 Hz, or phasic firing, where the constant firing rate is modulated by brief bursts (Grace, 2016; Grace and Bunney, 1984b, 1984a; Marinelli and McCutcheon, 2014). From this, we obtained DA time courses that clearly reflected the underlying neuronal firing patterns, exhibiting periods of tonic and phasic DA signaling, as well pauses where DA was cleared from the extracellular space (**Figure 1C**). Similar to naturally occurring DA transients measured in vivo (Robinson et al., 2002), maximal DA peaks were sub-micromolar (**Figure 1C**).

Next, we characterized the dopaminergic innervation of the striatum at a macroscale. To mimic the shape of the putamen in the human striatum, we modeled it as an ellipsoid. The dopaminergic innervation was constructed by filling the volume with axonal arbors from 10^5 SNc neurons, based on estimates from human SNc (Hardman et al., 2002) and the fact that dopaminergic SNc neurons have wide-spread projection targets (Poulin et al., 2018). Each neuron contributed to the dopaminergic innervation with a spherical arbor with a radius of 0.5 mm, wherein the density of terminals was constant (Doucet et al., 1986; Matsuda et al., 2009). As part of our analysis we investigated whether dopaminergic innervation was coherent (continuously overlapping) within the striatum, as defined by the

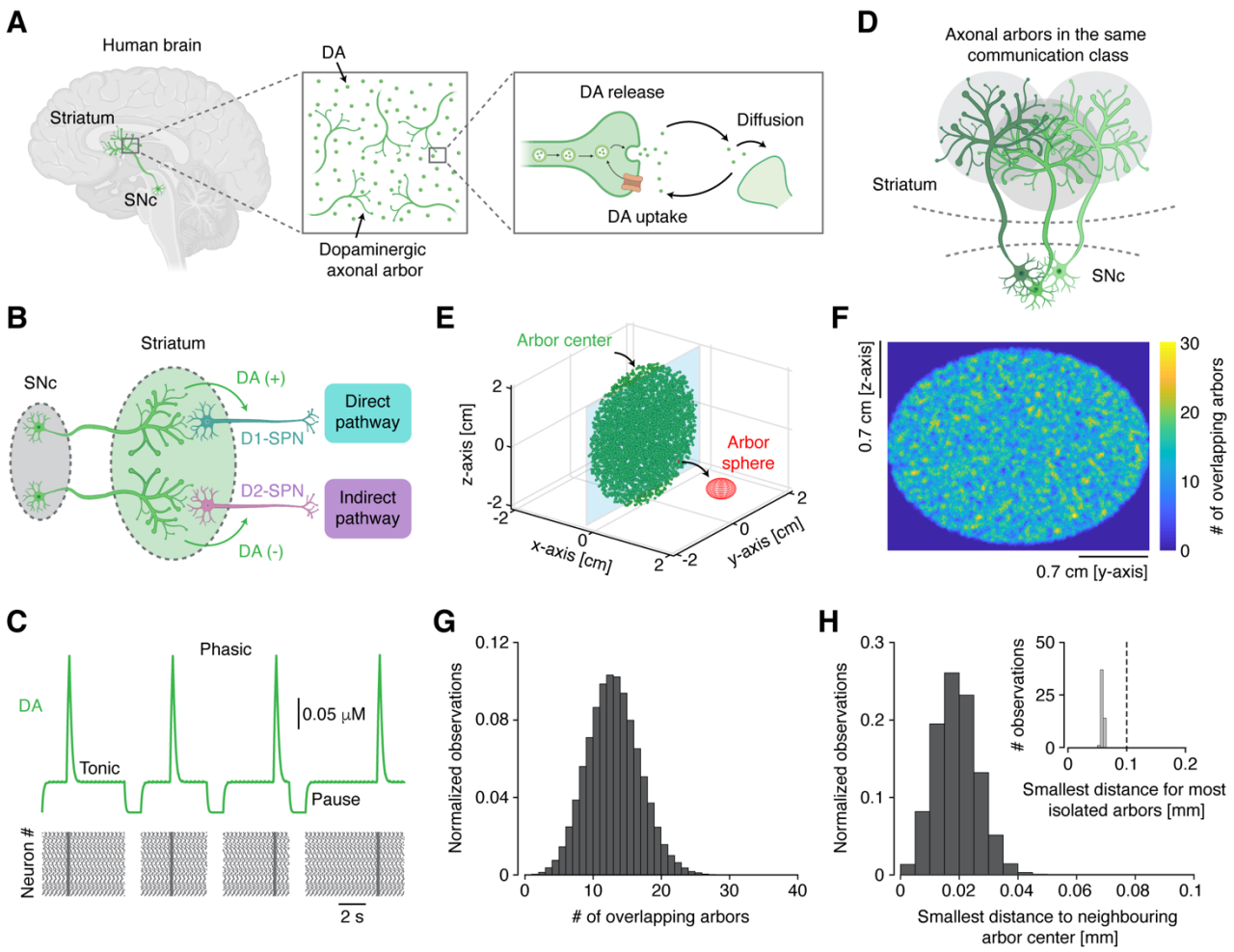

Figure 1. Functional and spatial characterization of DA signaling in the healthy human striatum. (A) Diagram of dopaminergic innervation and signaling in the human striatum. **(B)** Diagram of dopaminergic regulation of striatal D1- and D2-SPNs, parts of the direct and indirect pathway, respectively. **(C)** Example trace showing DA signaling and the underlying dopaminergic neuronal firing pattern. **(D)** Illustration of overlapping dopaminergic axonal arbors belonging to the same communication class. **(E)** Visualization of dopaminergic axonal arbors in the striatum; each arbor center is marked with a circle. For visibility, only 10% of arbors are shown. Red sphere shows the area subsumed by and arbor from one neuron. Notice that all arbors belong to the same communication class, represented by them all having the same color. **(F)** Heatmap of the distribution of overlapping arbors in the two-dimensional plane denoted in **(E)**. **(G)** Distribution of the number of overlapping arbors for each individual arbor. **(H)** Distribution of the smallest distance to the nearest neighboring arbor center for each individual arbor. Inset: Smallest distance to nearest neighboring arbor center for the most isolated arbors found using Voronoi tessellation.

number of communications classes. We assumed that dopaminergic neurons belonged to the same communication class if their arbors considerably overlapped (their arbor centers less than 0.5 mm apart; **Figure 1D**). Hence, if the number of communication classes is low, it would suggest a high degree of coherence and spatial coverage, and vice versa. We used an algorithm to classify neurons into communication classes (see Methods). We found that all neurons, in the healthy striatum, belonged to the same communication class (**Figure 1E**), suggesting a high degree of coherence and coverage (**Figure 1F**). For each dopaminergic neuron we counted the number of overlapping

arbors from other neurons. This metric followed a Poisson distribution (**Figure 1G**; see Supplementary Information [SI]). Next, we searched for spatially isolated areas in the striatum where the innervation was less dense, since such areas would be more susceptible to impairments in DA signaling during denervation. From calculations on the diffusion equation (see SI), we determined that points within the striatum with a distance larger than 0.1 mm to its nearest neighboring arbor could be defined as isolated. Using Monte Carlo simulations, we approximated the distribution of smallest distances (**Figure 1H**) and used Voronoi tessellation to find the most isolated points (**Figure 1H**; see SI). This showed that no isolated areas existed in the fully innervated, modelled striatum (**Figure 1H**). Overall, these results demonstrate that DA released in the healthy striatum exhibits three clearly distinct signaling periods: tonic, phasic and pauses. Furthermore, the dopaminergic arbors comprise a network that densely covers the entire striatum, where no isolated areas exist.

Different denervation patterns break down the dopaminergic network with distinct spatial and temporal evolutions

In biology, structure often informs function. Therefore, we next probed the spatial landscape of dopaminergic arbors in the denervating striatum. The subcellular pathways involved in the loss of dopaminergic neurons is a fundamental question beyond the scope of this study. Instead, we sought to characterize the structural properties of the remaining dopaminergic innervation arising from distinct models of progressive cell loss.

To describe dopaminergic denervation, we assumed that all neurons may have the same probability of death and neurons therefore die in a stochastic manner. We termed this model *random denervation* (RD; **Figure 2A**). In the second model, *prion-like denervation* (PLD), neurons die due to prion-based spreading (**Figures 2B**). This model was inspired by proposed mechanisms where protein aggregates spread between neurons and cause their degeneration (Chu and Kordower, 2015; Prusiner, 2012; Surmeier et al., 2017). For this, a small set of neurons were initially "infected", and at every timestep each infected neuron infected two neighboring neurons before being removed from the network. In the third model, *stress-induced denervation* (SID), neurons die due to oxidative cellular stress (Jenner, 2003; Sulzer, 2007) (**Figure 2C**). When dopaminergic neurons degenerate, the remaining neurons may upregulate their firing activity and DA synthesis in an attempt to maintain DA levels. However, dopaminergic neurons may already be close to their maximum metabolic capacity (Bolam and Pissadaki, 2012), and increased activity could thus trigger stress-induced cellular degeneration (Jenner, 2003; Sulzer, 2007). In this, we assumed that the pace by which a neuron dies is a function of the number of remaining neighbors; neurons with few overlapping arbors have a higher risk of dying compared to neurons with many overlapping arbors. These three models resulted in clearly distinct spatial landscapes, each characterized by a unique breakdown of the dopaminergic network. For RD, the remaining arbors covered the entire striatal space but no longer belonged to the same communication class (**Figure 2D**). Thus, the remaining innervation no longer formed a coherent network. In contrast, for PLD, large fractions of the striatum were deprived of arbors and instead dominated by one or two subregions with seemingly normal innervation (**Figure 2D**). For SID, arbors were concentrated in small, isolated microregions, each forming its own communication class (**Figure 2D**).

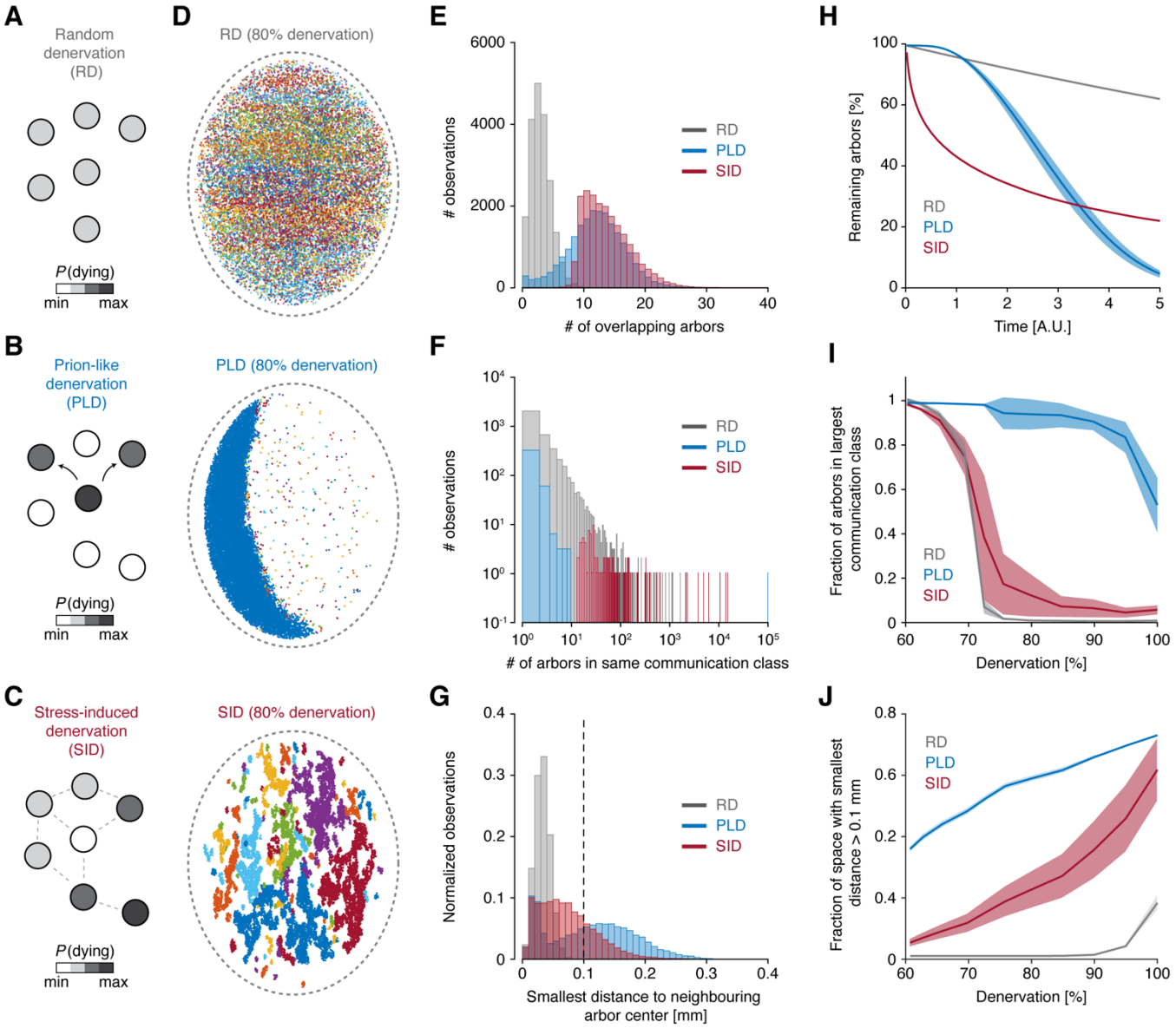

Figure 2. Different denervation patterns break down the dopaminergic network with distinct evolutions. (A) Diagram of network mechanism for random denervation (RD). The color of each dopaminergic neuron (circle) corresponds to probability of death. **(B)** Diagram of network mechanism for prion-like denervation (PLD). **(C)** Diagram of network mechanism for stress-induced denervation (SID). Doted lines denote overlap of arbors. **(D)** Visualization of the dopaminergic axonal arbor network following RD, PLD, and SID. Each color corresponds to a separate communication class. **(E)** Distributions of the number of overlapping arbors for each individual arbor at 80% denervation. **(F)** Distributions of the number of arbors in each separate communication class at 80% denervation. **(G)** Distributions of the smallest distance to the nearest neighboring arbor center for each individual arbor at 80% denervation. Dotted line denotes the threshold for classifying isolated areas. **(H)** Percentage of remaining arbors as a function of time. Full line is mean, and shading is standard deviation. **(I)** Fraction of arbors belonging to the largest communication class as a function of denervation. Full line is mean, and shading is standard deviation. **(J)** Fraction of striatal space with smallest distance to nearest arbor larger than 0.1 mm (isolated area) as a function of denervation. Full line is mean, and shading is standard deviation.

We next quantified these observations by the distribution of the number of overlapping axonal arbors in the denervated landscape (**Figure 2E**). As in the healthy striatum, the distribution for RD followed a Poisson distribution,

but with a significantly reduced mean value, and no arbors overlapped with more than 10 other arbors. For PLD, a notable fraction of arbors had very low numbers of overlapping arbors, whilst a large fraction had numbers similar to those in the healthy striatum (**Figure 2E**). In SID, only arbors with many overlapping neighbors remained and the distribution had a higher mean number of overlapping arbors compared to the healthy striatum (**Figure 2E**). This measure was determined from regions still containing some arbors and does thus not provide any direct information about the presence of isolated areas. Importantly, a commonality of all denervation models was, that at this stage, the dopaminergic network was broken down into multiple communication classes, but in distinct patterns (**Figure 2F**): RD had only small classes remaining, PLD contained many small but also one dominating class, whereas SID contained many classes containing 100 or more arbors. We also assessed the emergence of isolated areas (**Figure 2G**). For RD, no isolated areas existed. In contrast, for both PLD and SID, the striatum contained numerous isolated areas, deprived of arbors (**Figure 2G**).

We then followed key spatial characteristics as a function of denervation. First, we determined the percentage of remaining arbors as a function of time. For RD, this followed an exponential decay with a relatively slow temporal progression (**Figure 2H**). Interestingly, for PLD, the curve followed a convex function, suggesting that loss of dopaminergic neurons accelerated with time (**Figure 2H**). Conversely, the curve for SID followed a concave function, indicating that dopaminergic denervation in this scheme started fast, but then slowed with time (**Figure 2H**). These results have predictive strength and can be mathematically described by stretched exponentials on the form of: $N(t) \propto e^{-bt^c}$, with b being the decay rate and $c = 1$ for RD, $c > 1$ for PLD and $c < 1$ for SID. Next, we calculated the fraction of arbors in the largest communication class (**Figure 2I**). This measure equals one when all arbors are in the same communication class and goes to zero when all arbors are in different communication classes. PLD kept one dominating communication class until the final stage of denervation, while RD and SID were characterized by a tipping point, at which the network dramatically transitioned from fully coherent to segregated into multiple classes. Interestingly, this transition occurred around 75% denervation, correlating with when symptoms often present in patients (Bernheimer et al., 1973; Fearnley and Lees, 1991; Lee et al., 2000; Ma et al., 1997). Finally, for RD, we found no isolated areas before very severe denervation (>90%; **Figure 2J**). At 75% denervation, SID showed an increase in the fraction of isolated areas, with ~20% of the striatum being deprived of dopaminergic arbors. At the same denervation level, isolated areas comprised ~50% of the striatum in the PLD model. Overall, we found notable spatial and temporal differences between three distinct models of striatal dopaminergic denervation.

Distinct denervation patterns differentially effect local and global striatal SPN firing activity

The excitability of SPNs is strongly regulated by DA (Kreitzer, 2009; Kreitzer and Malenka, 2008; Lahiri and Bevan, 2020; Surmeier et al., 2007). Therefore, we next investigated how the different dopaminergic denervation patterns affected the activity of D1- and D2-SPNs. Previous work has shown that D1 and D2 receptors have low and DA affinity, respectively (Richfield et al., 1989) (**Figure 3A**). DA regulation of SPN excitability is mediated by the signaling molecule cyclic adenosine monophosphate (cAMP), produced downstream of DA receptors. D1 and D2 receptor activation increases and decreases the production of cAMP, respectively, and cAMP in turn regulates the activity of

a variety of ion channels in SPNs (Kreitzer, 2009; Kreitzer and Malenka, 2008) (**Figure 3A**). Inspired by previous work (Dreyer et al., 2010), we therefore described the intracellular cAMP concentration in D1- and D2-SPNs as:

$$\frac{dcAMP_{\mathrm{D1}}}{dt} = \alpha + \lambda_1 \frac{DA^h}{DA^h + \kappa_1^h} - \delta_1 cAMP_{\mathrm{D1}}$$

$$\frac{dcAMP_{\mathrm{D2}}}{dt} = \alpha + \lambda_2 \frac{\kappa_2^h}{DA^h + \kappa_2^h} - \delta_2 cAMP_{\mathrm{D2}}$$

Here α is the steady state production of cAMP and δ is the spontaneous decay of cAMP (see Methods). In addition, receptor-dependent cAMP production was implemented: cAMP production in D1- and D2-SPNs increased and decreased with DA stimulation, respectively. With increasing denervation, the cAMP production during phasic firing became progressively lower in D1-SPNs, whilst in D2-SPNs it became progressively lower during firing pauses (**Figures 3B** and **3C**). We next asked how these impairments manifest in the firing activity of SPNs. Using the Izhikevich model, we simulated the membrane potential of individual neurons with a stochastically varying synaptic current (Izhikevich, 2003), and assumed that the firing probability was as a function of cAMP levels (see Methods). For D1- and D2-SPNs we used the cAMP concentrations observed during dopaminergic phasic firing and firing pauses, respectively. This was motivated by the result that, in the healthy striatum, the highest cAMP production in D1- and D2-SPNs was observed during phasic firing and firing pauses, respectively (**Figure 3B**). In the healthy state, D1- and D2-SPNs fired vigorously during dopaminergic phasic firing and firing pauses, respectively (**Figure 3D**). However, in the denervated state, the activity of SPNs was dramatically affected. In D1-SPNs, the burst firing during dopaminergic phasic firing was greatly reduced, while in D2-SPNs the burst firing during dopaminergic firing pauses was almost abolished (**Figure 3D**). The observation that D2-SPNs were more severely affected than D1-SPNs is explained by cAMP concentrations decaying more rapidly in D2-SPNs compared to D1-SPNs (**Figure 3C**).

Next, we assessed the spatial effects on SPN firing activity as a function of the denervation pattern. To characterize the three denervation models, we spatially mapped the maximal D1-SPN firing rate during dopaminergic phasic firing, and maximal D2-SPN firing rate during firing pauses. In RD, although almost all subregions had relatively low DA levels compared with the healthy striatum, this was still enough to evoke intermediate D1-SPN firing activity across the extent of the striatum (**Figure 3E**). In contrast, in both PLD and SID, D1-SPN firing activity was high only in the remaining subregions with preserved DA innervation (**Figure 3E**). Noticeably, PLD transformed the striatum into a prominently polarized activity map, whereas SID caused local heterogeneity (**Figure 3E**). For D2-SPNs, the emergence of isolated areas, deprived of dopaminergic arbors, resulted in a very different outcome. Since the maximal DA concentration in isolated areas is zero (except for small diffusive fluctuations), D2-SPN firing rates were here very high, most profoundly expressed for PLD and SID (**Figure 3F**). We note here that, under actual physiological conditions, D2-SPNs residing in regions deprived of DA signaling might adapt by downregulating their firing activity to maintain homeostasis. In this scenario, the results would be similar to those for D1-SPNs. Finally, we characterized the global SPN activity in the three denervation models as a function of denervation level. The mean D1-SPN firing activity decreased linearly as a function of denervation in all models (**Figure 3G**). We also noted that the standard deviation of D1-SPN firing activity was notably smaller in RD compared

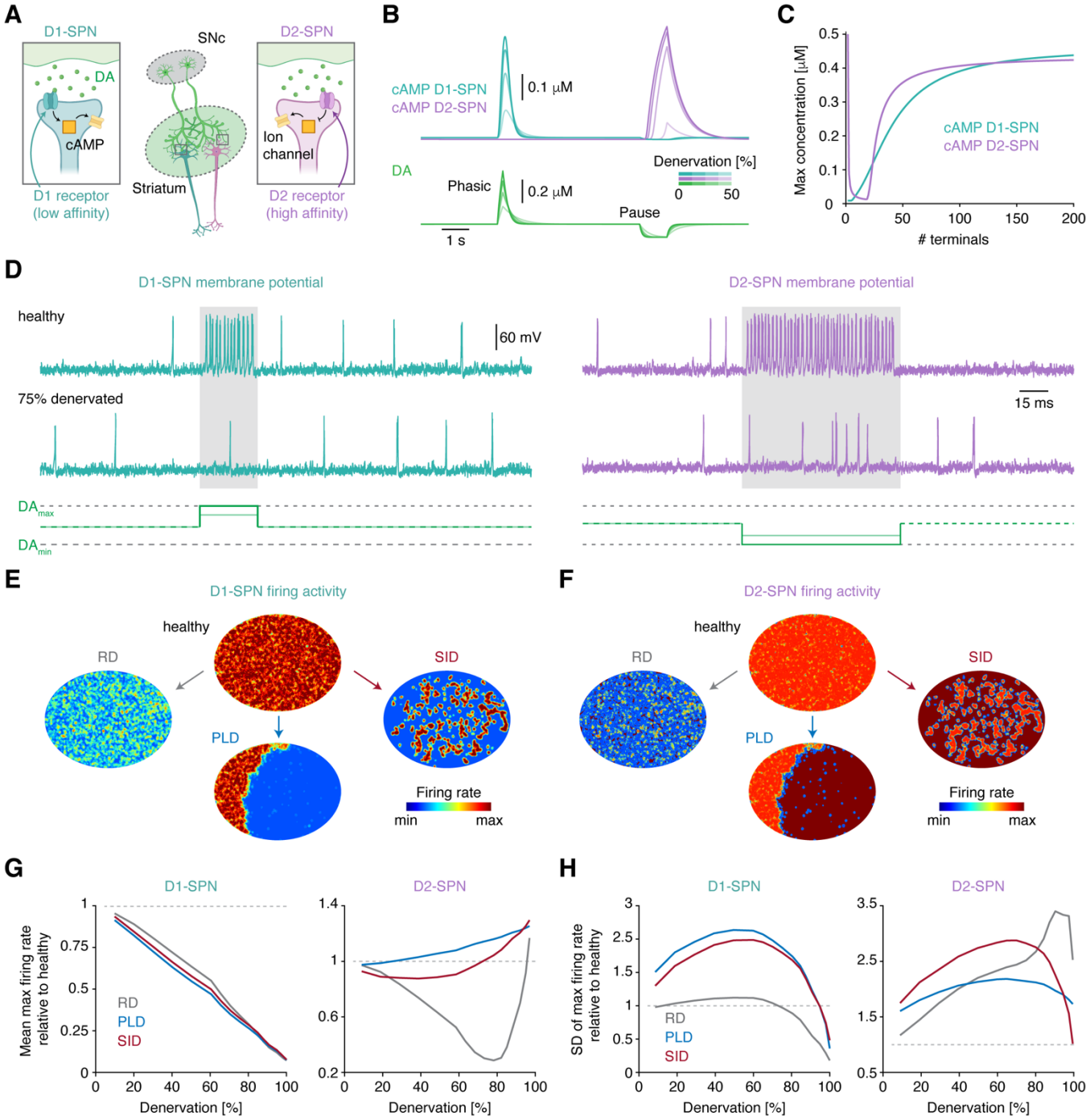

Figure 3. Distinct denervation patterns differentially effect local and global striatal SPN firing activity. (A) Diagram of how DA stimulates and inhibits, the production of cAMP in D1- and D2-SPNs, respectively. **(B)** Example traces showing cAMP in D1- and D2-SPNs as a function of DA signaling. **(C)** Maximal cAMP concentration in D1- and D2-SPNs during dopaminergic phasic firing and firing pauses, respectively, as a function of the number of dopaminergic terminals **(D)** Example traces showing the membrane potential of a D1-SPN and D2-SPN neuron in the healthy and 75% denervated striatum as a function of DA signaling. **(E)** Heatmap of the maximal D1-SPN firing activity across space in the healthy and 75 % denervated striatum for the three dopaminergic denervation patterns. **(F)** Same as in (E), but for D2-SPNs. **(G)** Spatial mean of maximum firing activity in D1- and D2-SPNs as a function of denervation. **(H)** Spatial standard deviation (SD) of maximum firing activity in D1- and D2-SPNs as a function of denervation.

to both PLD and SID, indicating spatial homogeneity of firing levels (**Figure 3H**). On the other hand, the effect on the mean D2-SPN firing activity was different: firing activity increased notably for PLD and slightly for SID, as a function denervation (**Figure 3G**). In RD, the firing activity decreased until it reached a minimum around 80% denervation, whereafter it rapidly increased (**Figure 3H**). This observation is explained by the co-occurrence of isolated areas, deprived of DA signaling, resulting in a dramatic increase in cAMP production in D2-SPNs (**Figure 3C**); in turn resulting in a profound increase in firing probability. Comparing the three models, it is clear that the early progression of denervation (up to ~60%) resulted in an increased standard deviation of SPN firing activity for all denervation patterns (**Figure 3H**). This increase in firing activity variance across neurons may be a fingerprint of the denervating striatum. Taken together, these results show that the local and global firing activity of D1- and D2-SPNs is strongly affected by the overall dopaminergic denervation level, but also by the specific spatial pattern of denervation.

A dual presynaptic compensation strategy preserves DA signaling in the denervated striatum

Given that dopaminergic neuron loss may trigger compensatory mechanisms in the remaining neurons in an attempt to maintain normal DA signaling (Brotchie and Fitzer-Attas, 2009; Zigmond, 1997), we sought to probe the potency of such mechanisms, in order to predict ideal therapeutic strategies. We included three compensatory mechanisms in our model and tested their impact on DA signaling. First, remaining dopaminergic terminals may increase their DA release capacity (Greenbaum et al., 2013; Zigmond, 1997; Zigmond et al., 1990). We refer to this as *enhanced release compensation* (ERC; **Figure 4A**):

$$\Gamma_+ \mapsto \frac{\Gamma_0}{1-\delta}$$

Here we have introduced the compensation parameter δ, a sigmoidal function going from zero to one as a function of the number of dopaminergic arbors covering a small volume. The parameter Γ_0, refers to the DA release in healthy subregions, whereas Γ_+ is the compensated release value. Second, DA transporters, expressed on dopaminergic terminals, may reduce their uptake capacity (Greenbaum et al., 2013; Lee et al., 2000; Zigmond, 1997; Zigmond et al., 1990). We refer to this as *decreased uptake compensation* (DUC; **Figure 4A**):

$$V_- \mapsto V_0(1-\delta)$$

As above, the parameter V_0, refers to the uptake value in healthy subregions, whereas V_- is the compensated uptake strength. Finally, we suggest a mechanism where neurons compensate by enhancing both DA release and uptake capacity in the terminals. Such a compensatory mechanism has not previously been suggested, and we refer to this as *dual enhanced compensation* (DEC; **Figure 4A**); included in the model through changes in both the uptake and release parameters:

$$V_+ \mapsto \frac{V_0}{1-\delta} \text{ and } \Gamma_+ \mapsto \frac{\Gamma_0}{1-\delta}$$

Here all parameters are defined as above. With these implementations, we simulated DA signaling and the corresponding cAMP production in D1- and D2-SPNs with a 50% denervation. As shown above, in the absence of any compensatory mechanism, DA release during tonic firing was unaffected, but notably affected during phasic firing and firing pauses; leading to impaired cAMP dynamics and abnormal firing in D1- and D2-SPNs (**Figures 3B** and **3D**). Here, during tonic firing, the DA concentration was notably increased for both ERC and DUC models; during phasic firing, DA was increased for ERC, and during firing pauses, DA removal was incomplete for DUC (**Figures 4B**). Importantly, the DEC model preserved DA levels during both tonic and phasic firing at the same levels as in the healthy state, while still allowing complete DA removal during firing pauses (**Figure 4B**). This suggests that a dual presynaptic compensation strategy – enhancing both DA release and uptake capacity – is required to counteract the negative effects on DA signaling dynamics caused by denervation.

Next we asked if any of the compensation mechanisms were able to ameliorate the impairments in SPN firing activity observed in the denervated state (**Figures 3B-H**). For this we calculated the spatial mean and standard deviation of the maximum D1- and D2-SPN firing rates in the three denervation models and combined these with implementation of the presynaptic compensation mechanisms. Interestingly, in the scenario of RD, only the DEC model preserved the mean level of D1- and D2-SPN firing activity (**Figure 4C**). In contrast, in the case of PLD and SID, neither of the three compensation models were able to counteract the drastic decrease in D1-SPN firing with denervation, whilst all models performed relatively well for D2-SPN activity (**Figures 4C**). Thus, in our models, it seems that normal levels of firing activity were maintained for both D1- and D2-SPNs only with the RD pattern combined with the DEC strategy. For the standard deviation of the D1-SPN firing activity, we note that in the RD scenario, all compensation models, as well as the no compensation model, maintained firing activity near the healthy level (**Figure 4D**). In contrast, for PLD and SID, the standard deviation was notably increased for all compensation models, and curiously, the non-compensated model was most similar to the healthy state (**Figure 4D**). For the standard deviation of the D2-SPN firing activity, none of the compensation models truly maintained this measure close to the healthy level, regardless of the denervation pattern (**Figure 4D**). It is here worth noting that the DEC model, across all denervation patterns, maintained the standard deviation of D2-SPN firing activity at a very low level (**Figure 4D**). This is because, in regions with low dopaminergic coverage, DA signaling from remaining terminals in the DEC model can compensate optimally, restoring coherent neuronal activity. The low standard deviation in firing activity across neurons means that all striatal subregions are capable of generating a very similar firing response upon dopaminergic stimulation. Overall, from these results, we conclude that the DEC model, in combination with the RD pattern, best preserved the global SPN firing activity, despite substantial denervation. In the final set of simulations, we explored this for all levels of denervation (**Figure 4E**). For the DEC model, the spatial mean firing activity of both D1- and D2-SPNs remained remarkably close to the healthy state, despite reaching severe denervation. In contrast, for the ERC and DUC models, even at relatively low denervation, the SPN firing activity differed from the healthy state. Specifically, around 50% denervation, the activity of D1- and D2-SPNs was notably higher and lower, respectively, compared to the healthy state. We speculate that especially the reduction in D2-SPN activity could cause motor side-effects by reducing the activity of the indirect pathway, relieving the suppression of

unwanted movements (Cui et al., 2013; Freeze et al., 2013; Kravitz et al., 2010; Kreitzer and Malenka, 2008). The ERC and DUC mechanisms do therefore not seem ideal as therapeutic strategies. Taken together, these results show that an ideal strategy to maintain normal SPN activity is to locally introduce a dual compensation mechanism – increasing both DA release and uptake capacity – and to globally minimize the dopaminergic arbor density differences, or at least avoid the emergence of isolated areas.

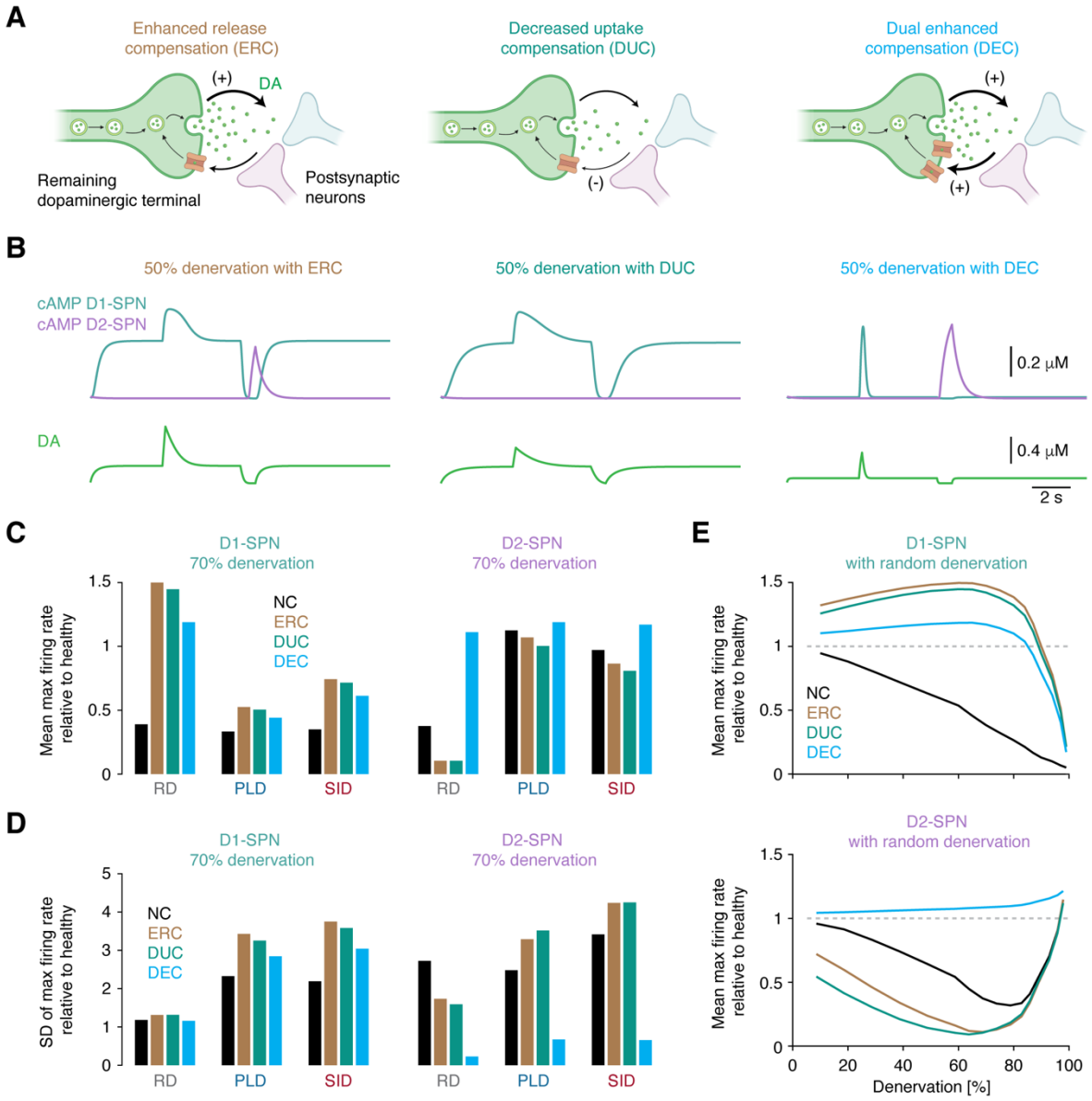

Figure 4. A dual presynaptic compensation strategy preserves DA signaling in the denervated striatum. (A) Diagrams of mechanisms of the enhanced release compensation (ERC), decreased uptake compensation (DUC), and dual enhanced compensation (DEC) models. **(B)** Example traces showing cAMP in D1- and D2-SPNs as a function of DA signaling at 50% denervation in the different models. **(C)** Spatial mean of maximum firing activity in D1- and D2-SPNs as a function of denervation pattern and compensation model. **(D)** Spatial standard deviation (SD) of maximum firing activity in D1- and D2-SPNs as a function of denervation pattern and compensation model. **(E)** Spatial mean of maximum firing activity in D1- and D2-SPNs as a function of denervation and compensation model in the randomly denervated striatum.

Discussion

Understanding the pathology of PD is a major challenge which requires contributions from different complementary scientific fields. In this work, we used biophysical modeling to investigate the spatial and functional landscape of dopaminergic signaling in the healthy and parkinsonian striatum. Our work provides three major insights and offers several experimentally testable predictions. First, we showed that the spatial pattern of dopaminergic denervation profoundly affects the structural and temporal breakdown of the dopaminergic network in the striatum. Second, both the local and global activity of D1- and D2-SPNs were differentially affected as a function of the spatial dopaminergic denervation pattern. Third, we identified that the optimal cellular strategy for maintaining normal striatal DA signaling, when neurons are progressively lost, is to enhance both DA release and uptake capacity.

Clinical variability in PD patients may be mediated by different dopaminergic denervation patterns

Typically, PD symptoms present when 60–80% of the dopaminergic neurons are lost (Fearnley and Lees, 1991; Ma et al., 1997). Still, the age of onset, disease progression and symptoms can vary notably between patients (Greenland et al., 2018; Lewis et al., 2005). Based on our results, we argue that the spatial pattern of dopaminergic denervation in the striatum, caused by different molecular mechanisms (Michel et al., 2016; Prusiner, 2012; Sulzer, 2007), could be a central determinant for much of this clinical variability. In this vein, clinical studies have shown that clinicians diagnose PD incorrectly in ~25% of patients (Tolosa et al., 2006); emphasizing the necessity for an applicable method to distinguish between PD, essential tremor, vascular parkinsonism, drug-induced parkinsonism and the atypical parkinsonian syndromes in the clinic. Importantly, the shape of the dopaminergic denervation curves varied remarkably depending on the denervation pattern. After an initial slow denervation rate, the loss of dopaminergic neurons accelerated with time in the PLD model. In contrast, in the SID model, denervation slowed with time after an initial rapid loss of dopaminergic neurons (**Figure 2**). The temporal evolution of the PLD and SID models correlate remarkably well with the clinical progression pattern seen in the early and middle stages of idiopathic PD and atypical parkinsonian syndromes, respectively (Eckert et al., 2007; Heijmans et al., 2019; Liu et al., 2015; Mcfarland, 2016; Payan et al., 2011). Our model thus predicts that the dopaminergic denervation pattern may be a central determinant for the disease progression variability and etiology seen in patients. In patients with RD, disease progression may be slow, whereas in patients with PLD, the progression may accelerate rapidly. Thus, if the total density of striatal dopaminergic terminals can be measured as a function of time in the early stages of the disease, it may be possible to determine the molecular mechanism and denervation pattern causing PD in individual patients. Furthermore, it may be possible to predict the time course of the disease progression, and from that determine the ideal therapeutic strategy for the individual patient. From our results, we therefore propose that future clinical experiments aim to measure the density of dopaminergic terminals in the striatum of PD patients over time, using for example single-photon emission computed tomography (Wang et al., 2012; Wszolek et al., 2015), and correlate this to disease progression. Combining the results from such experiments with biophysical modelling would elucidate the molecular and network mechanisms causing PD and disease variability.

We also found that the absolute time course of dopaminergic denervation was remarkably distinct between the different denervation patterns (**Figure 2**), and this observation could potentially aid clinicians in determining the differential diagnosis of parkinsonism. Clinical imaging of early-stage PD patients has shown that structural innervation differences in the striatum, albeit embracing a larger striatal area than our results, relates to different PD-related diseases. For example, large-scale asymmetry in striatal dopaminergic innervation associates with idiopathic parkinsonism (Kim et al., 2002; Ziebell et al., 2012), while large-scale symmetric denervation associates with atypical parkinsonian syndromes such as supranuclear palsy (Filippi et al., 2006; Knudsen et al., 2004; Varrone et al., 2001; Ziebell et al., 2012). This difference might be explained by the three denervation patterns in the model. Thus, the denervation curves from our model, in combination with high-resolution imaging, might portent a valuable tool for determining the pattern of clinical progression, and thus for distinguishing between different forms of parkinsonism in individual patients.

Distinct dopaminergic denervation patterns may differentially affect the direct- and indirect pathway

Locally, when dopaminergic terminals were lost, burst firing of D1- and D2-SPNs during dopaminergic phasic firing and firing pauses, respectively, was dramatically impaired (**Figure 3**). Given that D1- and D2-SPNs are critical components of the direct and indirect pathways, respectively, it is highly plausible that these two downstream pathways would be affected as a result (Kreitzer and Malenka, 2008). The reduction of burst firing in D1-SPNs during phasic dopaminergic firing would likely complicate the initiation of voluntary movements, whilst the lack of burst firing in D2-SPNs during dopaminergic firing pauses could cause unwanted, involuntary movements. Given that, in the denervated striatum, DA signaling and SPN activity varied across space in a manner depending on the spatial dopaminergic denervation pattern (**Figure 3**), we expect that different subregions of the striatum will have normal and abnormal activity of the direct and indirect pathways, depending on the dopaminergic denervation pattern. This may partially explain why disease symptoms vary notably between PD patients. We mention this with the caveat that D1- and D2-SPNs also communicate by lateral inhibition (Burke et al., 2017), and our simulations does not account for that. Furthermore, the striatum also contains local interneurons, whose axons never exit the striatum. We suggest that future work should aim at investigating the role of different dopaminergic denervation patterns in a more comprehensive network model of the striatum, as recently developed (Hjorth et al., 2020).

A dual cellular strategy maintains normal DA signaling and may delay severe symptoms in PD patients

Currently, no cure for PD exists and all available treatment strategies are aimed at alleviating symptoms. The most common pharmacological treatment is to administer levodopa, a precursor for DA, with the goal of increasing DA levels within the brain (Hauser, 2009). However, not all patients respond well to this treatment and it is associated with a range of side effects (Hauser, 2009). During the early stages of PD, it is thought that the loss of dopaminergic neurons is counterbalanced by endogenous compensatory mechanisms (Brotchie and Fitzer-Attas, 2009; Zigmond, 1997). Knowledge of such compensatory mechanisms could reveal potential targets for novel therapeutics for postponing and reducing the severity of PD symptoms (Brotchie and Fitzer-Attas, 2009). In this work, we found that DA signaling cannot be fully characterized by only the tonic, baseline DA level (**Figure 1**). The DA peaks during

phasic firing and the complete removal of DA during firing pauses are also an integral part of what we consider normal DA signaling in the healthy striatum, and likely plays important roles in proper neuronal signaling. Therefore, when evaluating the therapeutic potential of a cellular target, it is important to assess its effects on the full spectrum of DA signaling. Interestingly, the compensation strategy that best maintained normal striatal DA signaling, despite severe dopaminergic denervation, was a dual mechanism that enhanced both the release and uptake capacity of DA in the remaining neurons (**Figure 4**). In contrast to mechanisms that solely focused on increasing DA, such as enhanced DA release or suppressed DA uptake (**Figure 4**), this dual mechanism preserved the full DA signaling spectrum, without increasing baseline DA above levels observed in the healthy striatum. This suggests that cellular therapeutic strategies that achieve simultaneous enhancement of DA release and DA uptake capacity should be pursued. We speculate that this dual strategy would postpone the onset of severe symptoms by upholding normal DA signaling and may also cause less side effects compared to current pharmacological treatments, since baseline DA is maintained at a comparable level to in the healthy striatum (**Figure 4**).

Conclusion

PD is a highly debilitating disorder with complex and unknown etiology. Our work constitutes a new conceptual model for the clinical manifestations of PD, while providing a clear set of theoretical predictions and testable hypotheses. We regard our biophysical modeling and simulations as the first step towards further experimental investigations required to test our results. We expect these findings will lay the groundwork for new research directions within both basic and clinical sciences, aimed at better understanding, differentiating and hence treating PD.

Acknowledgements

We thank Ubadah Sabbagh and Eric Nicholas for critical comments on the manuscript. M.L.H. is grateful to Aleksandra Walczak and Thierry Mora for scientific discussions and valuable support. M.L.H. thanks Angela Taddei and Judith Mine-Hattab for encouragement and a fantastic scientific environment. M.L.H. and H.N.A. would like to thank Lene Oddershede for inspiration in the early stages of the project. R.R. acknowledge support from the Lundbeck Foundation (R230-2016-2326); M.H.J. acknowledge support from the Danish Council for Independent Research and StemPhys DNRF Center of Excellence (DNRF116).

Author contributions

M.L.H., H.N.A., M.H.J, J.K.D., and R.R. designed the research; M.L.H., and A.L. performed the research; M.L.H., H.N.A., A.L., J.K.D., and R.R. analyzed and interpreted the data; M.L.H., and R.R. made the figures; M.L.H., H.N.A., M.H.J., J.K.D., and R.R. wrote the paper.

References

Bernheimer, H., Birkmayer, W., Hornykiewicz, O., Jellinger, K., and Seitelberger, F. (1973). Brain dopamine and the syndromes of Parkinson and Huntington Clinical, morphological and neurochemical correlations. J. Neurol. Sci. *20*, 415–455.

Bolam, J.P., and Pissadaki, E.K. (2012). Living on the edge with too many mouths to feed: Why dopamine neurons die. Mov. Disord. *27*, 1478–1483.

Brotchie, J., and Fitzer-Attas, C. (2009). Mechanisms compensating for dopamine loss in early Parkinson disease. Neurology *72*, S32–S38.

Burke, D.A., Rotstein, H.G., and Alvarez, V.A. (2017). Striatal Local Circuitry: A New Framework for Lateral Inhibition. Neuron *96*, 267–284.

Chu, Y., and Kordower, J.H. (2015). The Prion Hypothesis of Parkinson's Disease. Curr. Neurol. Neurosci. Rep. *15*, 28.

Cui, G., Jun, S.B., Jin, X., Pham, M.D., Vogel, S.S., Lovinger, D.M., and Costa, R.M. (2013). Concurrent activation of striatal direct and indirect pathways during action initiation. Nature *494*, 238–242.

Damier, P., Hirsch, E.C., Agid, Y., and Graybiel, A.M. (1999). The substantia nigra of the human brain. II. Patterns of loss of dopamine-containing neurons in Parkinson's disease. Brain *122*, *Pt 8*, 1437–1448.

Doucet, G., Descarries, L., and Garcia, S. (1986). Quantification of the dopamine innervation in adult rat neostriatum. Neuroscience *19*, 427–445.

Dreyer, J.K. (2014). Three Mechanisms by which Striatal Denervation Causes Breakdown of Dopamine Signaling. J. Neurosci. *34*, 12444–12456.

Dreyer, J.K., Herrik, K.F., Berg, R.W., and Hounsgaard, J.D. (2010). Influence of Phasic and Tonic Dopamine Release on Receptor Activation. J. Neurosci. *30*, 14273–14283.

Eckert, T., Tang, C., and Eidelberg, D. (2007). Assessment of the progression of Parkinson's disease: a metabolic network approach. Lancet Neurol. *6*, 926–932.

Fearnley, J.M., and Lees, A.J. (1991). Ageing and Parkinson's disease: substantia nigra regional selectivity. Brain *114*, *Pt 5*, 2283–2301.

Filippi, L., Manni, C., Pierantozzi, M., Brusa, L., Danieli, R., Stanzione, P., and Schillaci, O. (2006). 123I-FP-CIT in progressive supranuclear palsy and in parkinson's disease: a SPECT semiquantitative study. Nucl. Med. Commun. *27*, 381–386.

Freeze, B.S., Kravitz, A. V., Hammack, N., Berke, J.D., and Kreitzer, A.C. (2013). Control of Basal Ganglia Output by Direct and Indirect Pathway Projection Neurons. J. Neurosci. *33*, 18531–18539.

Gillespie, D.T. (1977). Exact stochastic simulation of coupled chemical reactions. J. Phys. Chem. *81*, 2340–2361.

Grace, A.A. (2016). Dysregulation of the dopamine system in the pathophysiology of schizophrenia and depression. Nat. Rev. Neurosci. *17*, 524–532.

Grace, A.A., and Bunney, B.S. (1984a). The control of firing pattern in nigral dopamine neurons: single spike firing. J. Neurosci. *4*, 2866–2876.

Grace, A.A., and Bunney, B.S. (1984b). The control of firing pattern in nigral dopamine neurons: burst firing. J. Neurosci. *4*, 2877–2890.

Graybiel, A.M., and Grafton, S.T. (2015). The striatum: where skills and habits meet. Cold Spring Harb. Perspect. Biol. *7*, a021691.

Greenbaum, L., Lorberboym, M., Melamed, E., Rigbi, A., Barhum, Y., Kohn, Y., Khlebtovsky, A., Lerer, B., and Djaldetti, R. (2013). Perspective: Identification of genetic variants associated with dopaminergic compensatory mechanisms in early Parkinson's disease. Front. Neurosci. *7*, 52.

Greenland, J.C., Williams-Gray, C.H., and Barker, R.A. (2018). The clinical heterogeneity of Parkinson's disease and its therapeutic implications. Eur. J. Neurosci.

Hardman, C.D., Henderson, J.M., Finkelstein, D.I., Horne, M.K., Paxinos, G., and Halliday, G.M. (2002). Comparison of the basal ganglia in rats, marmosets, macaques, baboons, and humans: volume and neuronal number for the output, internal relay, and striatal modulating nuclei. J. Comp. Neurol. *445*, 238–255.

Hauser, R.A. (2009). Levodopa: Past, Present, and Future. Eur. Neurol. *62*, 1–8.

Heijmans, M., Habets, J.G.V., Herff, C., Aarts, J., Stevens, A., Kuijf, M.L., and Kubben, P.L. (2019). Monitoring Parkinson's disease symptoms during daily life: a feasibility study. Npj Park. Dis. *5*, 1–6.

Hirtz, D., Thurman, D.J., Gwinn-Hardy, K., Mohamed, M., Chaudhuri, A.R., and Zalutsky, R. (2007). How common are the "common" neurologic disorders? Neurology *68*, 326–337.

Hjorth, J.J.J., Kozlov, A., Carannante, I., Frost Nylén, J., Lindroos, R., Johansson, Y., Tokarska, A., Dorst, M.C., Suryanarayana, S.M., Silberberg, G., et al. (2020). The microcircuits of striatum in silico. Proc. Natl. Acad. Sci. U. S. A.

Izhikevich, E.M. (2003). Simple model of spiking neurons. IEEE Trans. Neural Networks *14*, 1569–1572.

Jenner, P. (2003). Oxidative stress in Parkinson's disease. Ann. Neurol. *53*, S26–S38.

Kim, Y.J., Ichise, M., Ballinger, J.R., Vines, D., Erami, S.S., Tatschida, T., and Lang, A.E. (2002). Combination of dopamine transporter and D2 receptor SPECT in the diagnostic evaluation of PD, MSA, and PSP. Mov. Disord. *17*, 303–312.

Knudsen, G.M., Karlsborg, M., Thomsen, G., Krabbe, K., Regeur, L., Nygaard, T., Videbæk, C., and Werdelin, L. (2004). Imaging of dopamine transporters and D2 receptors in patients with Parkinson's disease and multiple system atrophy. Eur. J. Nucl. Med. Mol. Imaging *31*, 1631–1638.

Kravitz, A. V., Freeze, B.S., Parker, P.R.L., Kay, K., Thwin, M.T., Deisseroth, K., and Kreitzer, A.C. (2010). Regulation of parkinsonian motor behaviours by optogenetic control of basal ganglia circuitry. Nature *466*, 622–626.

Kreitzer, A.C. (2009). Physiology and Pharmacology of Striatal Neurons. Annu. Rev. Neurosci. *32*, 127–147.

Kreitzer, A.C., and Malenka, R.C. (2008). Striatal plasticity and basal ganglia circuit function. Neuron *60*, 543–554.

Lahiri, A.K., and Bevan, M.D. (2020). Dopaminergic Transmission Rapidly and Persistently Enhances Excitability of D1 Receptor-Expressing Striatal Projection Neurons. Neuron *106*, 277-290.e6.

Lee, C.S., Samii, A., Sossi, V., Ruth, T.J., Schulzer, M., Holden, J.E., Wudel, J., Pal, P.K., de la Fuente-Fernandez, R., Calne, D.B., et al. (2000). In vivo positron emission tomographic evidence for compensatory changes in presynaptic dopaminergic nerve terminals in Parkinson's disease. Ann. Neurol. *47*, 493–503.

Lewis, S.J.G., Foltynie, T., Blackwell, A.D., Robbins, T.W., Owen, A.M., and Barker, R.A. (2005). Heterogeneity of Parkinson's disease in the early clinical stages using a data driven approach. J. Neurol. Neurosurg. Psychiatry *76*, 343–348.

Lippert, R.N., Cremer, A.L., Edwin Thanarajah, S., Korn, C., Jahans-Price, T., Burgeno, L.M., Tittgemeyer, M., Brüning, J.C., Walton, M.E., and Backes, H. (2019). Time-dependent assessment of stimulus-evoked regional dopamine release. Nat. Commun. *10*, 336.

Liu, Y., Fan, J.H., Gao, X., Ma, L., Qiao, Y.L., and Zhang, L. (2015). The natural progression of Parkinson's disease in a small cohort with 15 drug-naïve patients. Chin. Med. J. (Engl). *128*, 1761–1764.

Ma, S.Y., Röyttä, M., Rinne, J.O., Collan, Y., and Rinne, U.K. (1997). Correlation between neuromorphometry in the substantia nigra and clinical features in Parkinson's disease using disector counts. J. Neurol. Sci. *151*, 83–87.

Marinelli, M., and McCutcheon, J.E. (2014). Heterogeneity of dopamine neuron activity across traits and states. Neuroscience *282*, 176–197.

Matsuda, W., Furuta, T., Nakamura, K.C., Hioki, H., Fujiyama, F., Arai, R., and Kaneko, T. (2009). Single nigrostriatal dopaminergic neurons form widely spread and highly dense axonal arborizations in the neostriatum. J. Neurosci. *29*, 444–453.

Mazzoni, P., Hristova, A., and Krakauer, J.W. (2007). Why Don't We Move Faster? Parkinson's Disease, Movement Vigor, and Implicit Motivation. J. Neurosci. *27*, 7105–7116.

Mcfarland, N.R. (2016). Diagnostic Approach to Atypical Parkinsonian Syndromes. Contin. Lifelong Learn. Neurol. *22*, 1117–1142.

Michel, P.P., Hirsch, E.C., and Hunot, S. (2016). Understanding Dopaminergic Cell Death Pathways in Parkinson Disease. Neuron *90*, 675–691.

Paladini, C.A., Robinson, S., Morikawa, H., Williams, J.T., and Palmiter, R.D. (2003). Dopamine controls the firing pattern of dopamine neurons via a network feedback mechanism. Proc. Natl. Acad. Sci.

Panigrahi, B., Martin, K.A., Li, Y., Graves, A.R., Vollmer, A., Olson, L., Mensh, B.D., Karpova, A.Y., and Dudman, J.T.

(2015). Dopamine Is Required for the Neural Representation and Control of Movement Vigor. Cell *162*, 1418–1430.

Patriarchi, T., Cho, J.R., Merten, K., Howe, M.W., Marley, A., Xiong, W.-H., Folk, R.W., Broussard, G.J., Liang, R., Jang, M.J., et al. (2018). Ultrafast neuronal imaging of dopamine dynamics with designed genetically encoded sensors. Science (80-.). *360*, eaat4422.

Payan, C.A.M., Viallet, F., Landwehrmeyer, B.G., Bonnet, A.M., Borg, M., Durif, F., Lacomblez, L., Bloch, F., Verny, M., Fermanian, J., et al. (2011). Disease severity and progression in progressive supranuclear palsy and multiple system atrophy: Validation of the NNIPPS - PARKINSON PLUS SCALE. PLoS One *6*.

Poulin, J.-F., Caronia, G., Hofer, C., Cui, Q., Helm, B., Ramakrishnan, C., Chan, C.S., Dombeck, D.A., Deisseroth, K., and Awatramani, R. (2018). Mapping projections of molecularly defined dopamine neuron subtypes using intersectional genetic approaches. Nat. Neurosci. *21*, 1260–1271.

Prusiner, S.B. (2012). A Unifying Role for Prions in Neurodegenerative Diseases. Science (80-.). *336*, 1511–1513.

Richfield, E.K., Penney, J.B., and Young, A.B. (1989). Anatomical and affinity state comparisons between dopamine D1 and D2 receptors in the rat central nervous system. Neuroscience *30*, 767–777.

Robinson, D.L., Heien, M.L.A. V, and Wightman, R.M. (2002). Frequency of dopamine concentration transients increases in dorsal and ventral striatum of male rats during introduction of conspecifics. J. Neurosci. *22*, 10477–10486.

Rodriguez-Oroz, M.C., Jahanshahi, M., Krack, P., Litvan, I., Macias, R., Bezard, E., and Obeso, J.A. (2009). Initial clinical manifestations of Parkinson's disease: features and pathophysiological mechanisms. Lancet Neurol. *8*, 1128–1139.

Sulzer, D. (2007). Multiple hit hypotheses for dopamine neuron loss in Parkinson's disease. Trends Neurosci. *30*, 244–250.

Surmeier, D.J., Ding, J., Day, M., Wang, Z., and Shen, W. (2007). D1 and D2 dopamine-receptor modulation of striatal glutamatergic signaling in striatal medium spiny neurons. Trends Neurosci. *30*, 228–235.

Surmeier, D.J., Obeso, J.A., and Halliday, G.M. (2017). Selective neuronal vulnerability in Parkinson disease. Nat. Rev. Neurosci. *18*, 101–113.

Tolosa, E., Wenning, G., and Poewe, W. (2006). The diagnosis of Parkinson's disease. Lancet Neurol. *5*, 75–86.

Varrone, A., Marek, K.L., Jennings, D., Innis, R.B., and Seibyl, J.P. (2001). [123I]β-CIT SPECT imaging demonstrates reduced density of striatal dopamine transporters in Parkinson's disease and multiple system atrophy. Mov. Disord. *16*, 1023–1032.

Wang, L., Zhang, Q., Li, H., and Zhang, H. (2012). SPECT molecular imaging in Parkinson's disease. J. Biomed. Biotechnol. *2012*, 412486.

Wszolek, Z.K., Ba, F., and Martin, W.R.W. (2015). Dopamine transporter imaging as a diagnostic tool for parkinsonism and related disorders in clinical practice. Park. Relat. Disord. *21*, 87–94.

Ziebell, M., Andersen, B.B., Thomsen, G., Pinborg, L.H., Karlsborg, M., Hasselbalch, S.G., and Knudsen, G.M. (2012). Predictive value of dopamine transporter SPECT imaging with [123I]PE2I in patients with subtle parkinsonian symptoms. Eur. J. Nucl. Med. Mol. Imaging *39*, 242–250.

Zigmond, M.J. (1997). Do Compensatory Processes Underlie the Preclinical Phase of Neurodegenerative Disease? Insights from an Animal Model of Parkinsonism. Neurobiol. Dis. *4*, 247–253.

Zigmond, M.J., Abercrombie, E.D., Berger, T.W., Grace, A.A., and Stricker, E.M. (1990). Compensations after lesions of central dopaminergic neurons: some clinical and basic implications. Trends Neurosci. *13*, 290–296.

Methods

Resource availability

Lead Contact

Further information and requests for resources should be directed to and will be fulfilled by the Lead Contact, Rune Rasmussen (runerasmussen@dandrite.au.dk).

Materials availability

This study did not generate new unique reagents.

Data and code availability

All code is made publicly available at the GitHub repository:
https://github.com/Mathiasheltberg/Theoretical_Denervation_ParkinsonsModel.

Method details

Simulations in the mean-field model

To construct the mean field model, we considered a cubic volume of dimensions 10 μm x 10 μm x 10 μm. Since the density of dopaminergic axonal terminals is estimated to be $0.1/\mu m^3$, this volume contained 100 terminals. Next we considered the diffusion coefficient being $D \approx 380\ \mu m^2/s$, and thus the time for DA to equilibrate would be $\Delta t \approx \frac{(\Delta x)^2}{2D} \approx 0.03$ s, with $\Delta x = 5$ μm. We therefore performed the simulations with this timestep and assumed that a release of DA would affect the DA level in the entire volume. We also assumed that the influx from neighboring axonal arbors, would be equal to the outflux, since the density of dopaminergic terminals would be homogenous on these small length scales.

Simulation of the spatial dopaminergic network

To construct the dopaminergic network, we considered each dopaminergic axonal arbor to be a sphere, with its coordinate centrum defined by three random numbers *(cx, cy, cz):*

$$(\frac{cx}{a})^2 + (\frac{cy}{b})^2 + (\frac{cz}{c})^2 \leq 1$$

where *a*, *b* and *c* are the principal axes of the ellipsoid defining the striatum in the model. Having placed these spheres, we generated a connected network, where we let two dopaminergic neurons interact if the distance between the two arbor centers was less than or equal to the radius of one arbor.

Defining communication classes

We considered the communication classes of the dopaminergic network by defining that two neurons, *i* and *j*, communicate if there is a possible path from *i* to *j*. This means that they do not need to be directly functionally connected, but they should indirectly be able to transmit information between each other. If the dopaminergic neurons communicate, we defined the network to be irreducible. To find the communication classes we devised the following algorithm:

1) Pick neuron n_1 and put it in set S_1.
2) Find all its axonal arbor neighbors and put these in a transient set C = $\{n_j....n_k\}$.
3) Pick the first element of C, put it in S_1, remove it from C, and find all its neighboring arbors and put these in C.
4) Pick the next element of C and repeat the algorithm. When C is empty, S_1 is a collection of all arbors in communication class 1.
5) After this, take n_2. If $n_2 \in S_1$ go to n_3. Otherwise create set S_2, put all the connections of n_2 in C, and repeat the algorithm as above.

Removing dopaminergic neurons

To simulate the dopaminergic denervation of the striatum we compared three algorithms that emulate three distinct molecular mechanisms (i.e. random, prion-like, and stress-induced) causing neurons to die. Fundamentally, all were algorithms were event-driven Gillespie algorithms (Gillespie, 1977), in that the time of the next event was chosen by:

$$t_{next} = t - \frac{ln(rand)}{\sum_i^N \lambda \mathrm{i}}$$

And the neuron *x*, that was chosen to die, was selected by fulfilling the criteria:

$$\sum_j^x \lambda \mathrm{j} \sum \mathrm{iN} \lambda \mathrm{i}$$

The defined rates differed fundamentally between the three models are explained below:

1) Random denervation (RD): At time t = 0, all dopaminergic neurons are considered to have the same probability to die. This means that they all have a constant rate, and therefore $\lambda_i = \lambda_0$. This leads to an exponential decay in the number of remaining neurons per time.

2) Prion-like denervation (PLD): At time t = 0, a dopaminergic neuron is infected and will die with rate λ_0. This updates the time, and before it dies, it passes on the infection to two neighboring neurons, if there exist two neighbors that are not yet infected. Next , one of these will be chosen, so $t_{next} = t - \frac{ln(rand)}{N_I \lambda_0}$, where N_I is the number of infected neurons. This will lead to a decrease in the time between events, and thus an accelerating denervation process.

3) Stress-induced denervation (SID): At time t = 0, all dopaminergic neurons have a rate to die depending on the number of overlapping axonal arbors, n_i, in the network. Therefore we define the rate as a logistic function given by: $\lambda_i = \lambda_0 \frac{e^{-\beta(n_i-\gamma)}}{1+e^{-\beta(n_i-\gamma)}}$. Here γ is the threshold value, typically chosen to be 15 since this is approximately half the number found in the healthy striatum and β is the steepness, typically chosen to be 10. This function generates a decelerating pattern as the most vulnerable dopaminergic neurons die initially.

SPN firing activity

To model the SPN (D1 and D2) firing activity, we used a previously proposed spiking neuron model (Izhikevich, 2003). This model is inspired, by the more computationally complex Hodgkin-Huxley models, but generates similar neuronal dynamics. Thus, it is a minimal model, where the combination of different parameters can generate different neuronal firing patterns, such as tonic or burst firing. Thus, we described the membrane potential dynamics of D1- and D2-SPNs, taking the cAMP level into account, through two coupled differential equations:

$$\frac{dv}{dt} = 0.04v^2 + 5v + 140 - u + I$$

$$\frac{du}{dt} = a(bu - v) \text{ where } b = b_0 + cAMP_{D_i}$$

With the reset condition:

$$\text{if } v \geq 30 \text{ mV} \Rightarrow \begin{Bmatrix} u = u + d \\ v = c \end{Bmatrix}$$

In this model, v and u are dimensionless parameters, dv represents the membrane potential of the SPN, and du represents a membrane potential recovery variable, which accounts for the activation of K^+ currents and the inactivation of the Na^- currents. Thereby u provides a negative feedback to v. Furthermore, synaptic currents implemented through the variable I. In this model, the effect of cAMP on neuronal excitability is implemented in the simplest way. The cAMP molecules are thought to regulate neuronal excitability by modulating the conductance of different ion channels situated in the membrane on the neuron. This model thus implements a natural way to model this interplay. From our description, a higher level of cAMP increases the firing probability in the neuron, thus triggering more action potentials when stimulated with a synaptic current.

Software

All simulations were performed in MATLAB (Mathworks). Figures were assembled using Illustrator (Adobe), and schematic diagrams created using BioRender.

Table 1. Overview of parameters used for simulations.

Structural parameters	
Size of subvolume	10 x 10 x 10 = 1000 μm^3
Size of striatum (axes)	0.3 cm 1.5 cm 2.1 cm
Size of striatum (volume)	4 x π/3 x (0.3 x1.5 x 2.1) = 3.96 cm^3
Axonal arbor of neuron (radius)	0.5 mm
Axonal arbor of neuron (volume)	4 x π/3 x 0.05^3 = 0.54 mm^3
Number of neurons projecting into healthy striatum	10^5
Diffusion coefficient in striatum	380 μm^2/s
Dopaminergic neuron firing parameters	
Δ (release per terminal)	0.0025 μM
V_M (uptake per terminal)	0.041 μM/s
ν (firing frequency [tonic])	4 Hz
ν (firing frequency [pause])	0 Hz
ν (firing frequency [phasic])	15 Hz
ν (degradation of dopamine)	0.04/s
K_M (Michaelis-Menten parameter)	0.21 μM
cAMP production parameters	
α (constant production)	0.001 μM/s (D1-SPN) 0.001 μM/s (D2-SPN)
λ (receptor stimuli dependent production)	5.0 (D1-SPN) 1.0 (D2-SPN)
κ (affinity)	0.25 (D1-SPN) 0.0025 (D2-SPN)
h (Hill coefficient)	4 (D1-SPN) 4 (D2-SPN)
δ (active cAMP degradation)	10/s (D1-SPN) 2/s (D2-SPN)

D1- and D2-SPN firing parameters (dimensionless units)	
a (decay rate for u)	0.05
b_0 (sensitivity)	0.2
c (reset value for v)	-45 to -30
d (reset value for u)	5